GUIDED-MODE RESONANCE DEVICES: OMNIDIRECTIONAL REFLECTORS, WIDEBAND ABSORBERS, SENSORS AND NARROWBAND FILTERS

by

WENHUA WU

Presented to the Faculty of the Graduate School of
The University of Texas at Arlington in Partial Fulfillment
of the Requirements
for the Degree of

MASTER OF SCIENCE IN ELECTRICAL ENGINEERING

THE UNIVERSITY OF TEXAS AT ARLINGTON

December 2011

ACKNOWLEDGEMENTS

I am deeply grateful to my supervising professor, Dr. Robert Magnusson, for his competent guidance and patient help during the past two years. His conscientious attitude towards work exerts a subtle and positive influence on me. I also would like to thank my graduate committee members Dr. Mingyu Lu, Dr. Weidong Zhou and Dr. Michael Vasilyev for their help and valuable comments.

I have been feeling glad and fortunate to work in Nanophotonics Device Group, where I have the opportunity for collaborating on various interesting projects with other brilliant researchers. I would like to thank Dr. Jaewoong Yoon for his pertinent advices and collaboration on omnidirectional absorbers, Dr. Kyu J. Lee for working with me on experimental aspects of omnidirectional absorbers and reflectors, Debra Wawro and Shelby Zimmerman for our collaboration on resonant sensors. I am indebted to Huan Nguyen for helping me to fabricate devices, Dr. Yiwu Ding for collaborating on developing graphical user interface software, and Dr. Mehrdad Shokooh-Saremi for his kind training on codes and software. I also wish to acknowledge helps and encouragements from my colleagues Kristin Pearl, Tanzina Khaleque, Pei Yee Lim, Mohammad Jalal Uddin, Mohammad Shyiq Amin, Xin Wang, Guoliang Chen and Muhammad Haisam Javed.

My interest in nanophotonics has begun at the Wuhan National Laboratory for Optoelectronics, in the Silicon Photonics and Microsystems Research Group led by Dr. Zhiping Zhou, to whom I wish to express my sincere appreciation. I would also like to thank my former colleagues Dr. Huaming Wu, An Mao and Zhixuan Xia for introducing me into this area.

Finally, I would like to express my warmest gratitude to my parents, sisters and friends for their care and understanding.

November 15, 2011

ABSTRACT

GUIDED-MODE RESONANCE DEVICES: OMNIDIRECTIONAL REFLECTORS, WIDEBAND ABSORBERS, SENSORS AND NARROWBAND FILTERS

Wenhua Wu, M.S.

The University of Texas at Arlington, 2011

Supervising Professor: Robert Magnusson

In this thesis, a series of guided-mode resonance (GMR) devices are developed and optimized in the optical spectral region. Some of these devices are designed by inverse algorithms such as genetic algorithm and particle swarm optimization. One-dimensional subwavelength silicon and germanium gratings providing high omnidirectional reflectivity within specific band are designed respectively for TE and TM polarization. A simple amorphous silicon waveguide grating is proposed to enhance the absorbance for solar cells by 60% comparing with unpatterned structure. Another presented grating absorbs light nearly totally in the ~ 0.3-0.6 μm wavelength band for all incidence angles independent of polarization, namely wideband omnidirectional absorber. GMR photonic sensors are also discussed and demonstrated mainly on a post analysis method that can improve the testing accuracy. It is a back-fitting model that helps to differentiate the biochemical target from outside environmental disturbers. In addition, GMR filter showing extremely narrow linewidth ~10 pm is also presented.

TABLE OF CONTENTS

LIST OF ILLUSTRATIONS

CHAPTER 1

INTRODUCTION

1.1 Introduction

Guided-mode resonance (GMR) devices constitute a class of periodic elements that utilize a photonic modal resonance effect as a fundamental mechanism related applications include narrow/wide band bandstop/bandpass filters, reflectors, polarizers, biosensors, slow-light elements, leaky-mode nanoplasmonics, absorbance-enhanced solar cells and omnidirectional reflectors/absorbers [1]. Guided-mode resonance photonics provide a great application platform in various areas such as laser, optical communication, medicine, sensors for medical diagnostics, homeland security, and environmental monitoring.

Guided-mode resonance was historically recognized as one of the two types of dielectric grating anomalies associated with rapid variations in intensity on variation of incidence angle or wavelength. The other type is Rayleigh anomaly which is caused by one of the spectral orders becoming an evanescent wave inducing energy redistribution [2]. However, the resonant type, guided-mode resonance [3-10], is caused by guided complex waves supportable by the waveguide grating. In dielectric gratings, these guided waves are leaky waveguide modes that may result in total reflection of incident light in broad or narrow bands. This enables applications including broadband reflectors, omnidirectional reflectors and narrow linewidth filters. In metallic/dielectric gratings, the guided waves can be plasmonic modes and may lead to the total absorption of incident light. Recent studies show that even in pure dielectric gratings, total absorption within partial solar spectral band is realizable, which provides a promising method for enhancing absorbance in solar cells and omnidirectional absorption applications.

1.2 Overview of the Thesis

This work addresses several types of GMR devices: reflectors, absorbers, biosensors and extremely narrow filters. Before demonstrating the details of such devices, it is helpful to introduce simulation methods and design tools used in this thesis. Rigorous coupled-wave analysis (RCWA) [11] is used to do the forward calculation of the diffraction efficiency and plot field patterns. Inverse tools, incorporating particle swarm optimization (PSO) [12] and genetic algorithm (GA) [13, 14] into the core RCWA codes, are used for device design.

Chapter 2 discusses GMR reflectors, especially omnidirectional reflectors. One-dimensional subwavelength silicon and germanium gratings providing high omnidirectional reflectivity within specific band are designed respectively for TE and TM polarization [15]. In Chapter 3, the GMR absorption mechanism is discussed in detail. A simple amorphous silicon waveguide grating is proposed to enhance the absorbance for solar cells by 60%. Moreover, chapter 3 presents deep waveguide gratings absorbing light nearly totally in the ~ 0.3-0.6 μm wavelength band for all incidence angles independent of polarization, thus realizing a wideband omnidirectional absorber. Chapter 4 mainly demonstrates a post analysis method that can improve the accuracy of resonant photonic biosensors. It is a back-fitting model that differentiates the biochemical target from outside environmental disturbers. In chapter 5, a GMR filter showing extremely narrow linewidth ~9 pm is discussed. Finally, in the last chapter, the thesis is summarized and potential future work is discussed.

CHAPTER 2

OMNIDIRECTIONAL GMR REFLECTORS

2.1 Introduction

Optical reflectors can be considered as a type of optical filters whose main purpose is to reflect the incident wave as well as possible. Depending on the applications, additional features may be required such as broad frequency band, good angular tolerance, low absorption for high power laser applications, and omnidirectional reflection for LED applications.

Generally, there are two main types of reflectors: metallic and dielectric. The former is simpler but not necessarily with worse performance. Actually, metallic films like silver, gold and copper are quite good performers in the infrared (IR) and near infrared wavelengths. Another important advantage of metallic mirrors is the small dependence of the incident angle and polarization. However, the problem of high absorption appears when the wavelength goes to visible and ultraviolet (UV) light ranges. Even at IR wavelengths absorption is high enough to damage the mirror for high power laser applications.

As an alternative to metallic mirrors, multilayer dielectric coatings are often used [16]. The optical principle of multilayer dielectric reflectors is multiple beam interference. The classic design of such devices is alternating quarter-wave layers of two different materials. High reflectance is observed because the beams reflected from all the interfaces are in phase when they reach the last interface where the constructive interference occurs. This type of dielectric mirrors provides broadband and omnidirectional reflection; however, this generally requires many layers, sometimes even tens of layers.

Another sort of dielectric reflectors is based on guided-mode resonance [8-10]. One advantage of GMR reflectors is they have good performance comparable to multilayer structures but typically with only 1-3 layers. Ding and Magnusson reported a ~600nm band

reflector with only a single binary layer with one dimensional periodicity [8]. Shokooh-Saremi and Magnusson realized extremely broadband (2-3.2 μm) reflectors with three-level GMR structures [17]. Both designs have reached reflectance larger than 99%. As examples of devices in this thesis, two new wideband GMR TM-reflector designs are shown with silicon and silica substrate for comparison. As Figure 2.1 shows, the design using silicon substrate has better flatness and wider band than the one using silica substrate in this case.

Figure 2.1 shows high reflectivity, broadband wavelength band response and geometric simplicity of these GMR reflectors, but the angular tolerance is not very good. C Tsai reported omnidirectional reflector based on dual effect of GMR and surface plasmon resonance, combining dielectric material with metal [18]. To the author's knowledge, no omnidirectional reflectors using pure GMR effect in dielectric grating have been previously reported. In this chapter, omnidirectional GMR reflector examples will be presented for both transverse-electric (TE) and transverse-magnetic (TM) polarized light. In the whole thesis, we define that TE (TM) polarized input light has an electric (magnetic) field vector normal to the plane of incidence.

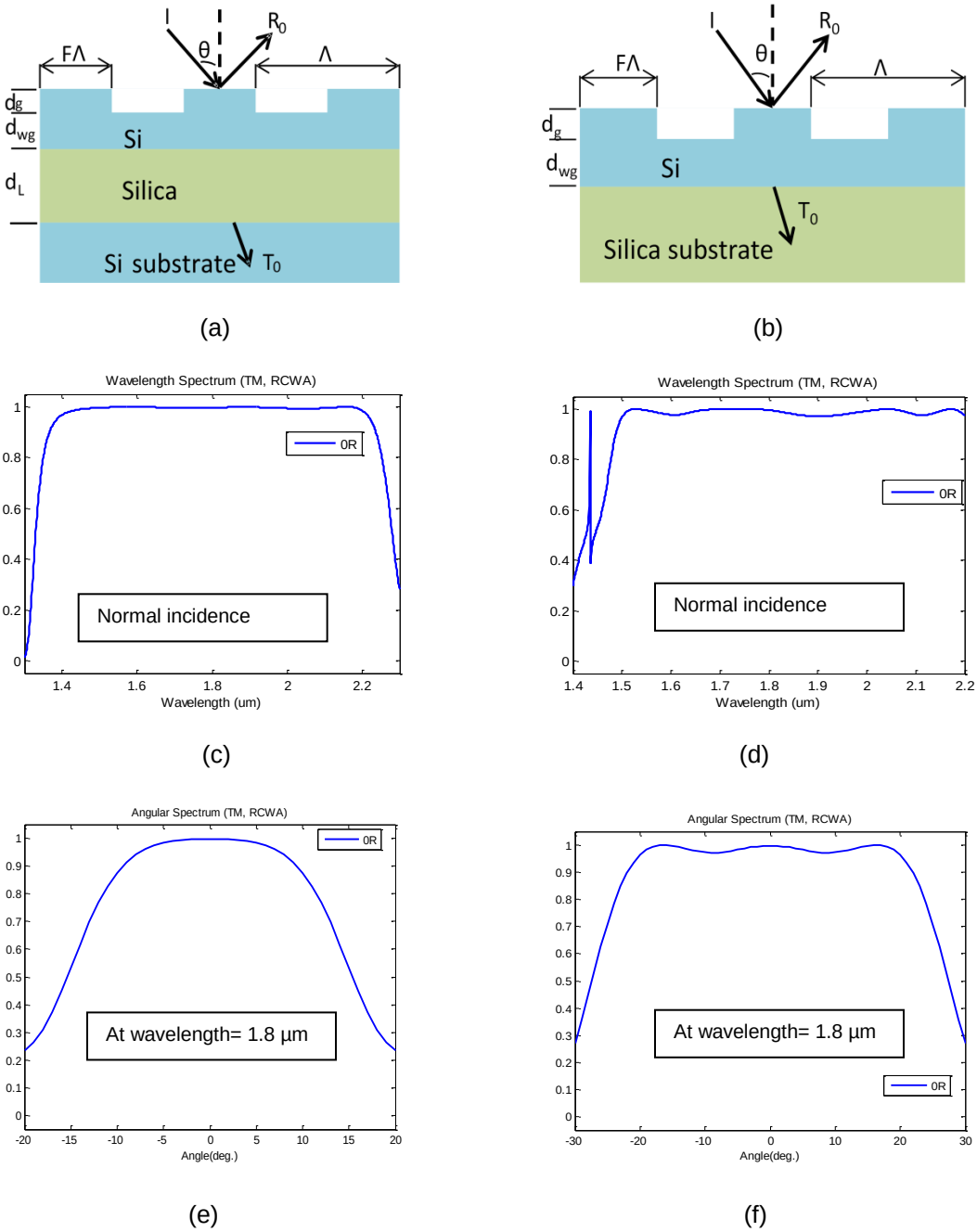

Figure 2.1 Wideband reflectors under TM polarization. The parameters of (a) are d_g= 484 nm, d_{wg}= 268 nm, d_L= 1222nm, Λ= 853nm, F= 0.655, and the corresponding wavelength spectrum (c) and angular spectrum (e) are shown. The parameters of (b) are d_g= 506 nm, d_{wg}= 821nm, Λ= 849 nm, F= 0.555, and the corresponding wavelength spectrum (d) and angular spectrum (f) are shown.

2.2 Omnidirectional Reflectors

Omnidirectional reflectors (ODRs) [19] are of interest for applications in optoelectronics, LED lighting [20-22], optical communications [23] and integrated optics [24]. In this section, the design of all-dielectric ODRs based on GMR in a simple waveguide grating is demonstrated.

The GMR device treated here consists of a subwavelength silicon grating on top of a silica substrate as shown in Figure 3.2. All the parameters including grating depth d_g, waveguide thickness d_{wg}, period Λ, and fill factor F are of importance for properly engineering the location, strength, and bandwidth of the resonances.

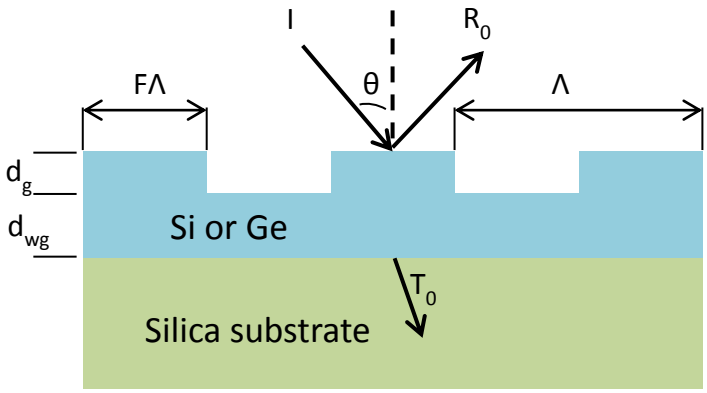

Figure 2.2 Schematic diagram of the GMR ODR. Here I denotes incident wave, R_0 is zero-order reflectance and T_0 is zero-order transmittance.

2.2.1. TE Omnidirectional Reflectors

In order to obtain profile parameters where the GMR structure works well for reflecting incident waves at all angles, a numerical genetic algorithm is applied in the design. When the center wavelength is set to be 2 μm under TE polarization using silicon, the returned parameters are d_g = 0.989 μm, d_{wg} = 0.15 μm, Λ = 0.816 μm and F = 0.573.

To see the performance of the structure with these parameters, RCWA is used to calculate the reflectance spectra as function of wavelength and angle [11, 25]. Figure 2.3 exhibits a computed reflectance map for zero-order reflectance R_0 (λ, θ), showing that the

device exhibits a bandwidth of approximately 50 nm in the wavelength band spanning 1.953–2.003 μm for which R_0 is high. Additional details for the reflectance spectra are provided in Figure 2.4, where the spectral variations of R_0 (λ, θ) at fixed example angles in this 50-nm band and at fixed example wavelength in all angles are shown. As exemplified in Figure 2.3, our computations show that the reflectance varies approximately in the range $0.9<R_0<1.0$ across the angular range $0^\circ < \theta < 89^\circ$ and in the spectral range spanning ~1.953 μm<λ<2.003 μm. Taking an angular average across this λ-θ rectangle gives an average reflectance R_0 >95%.

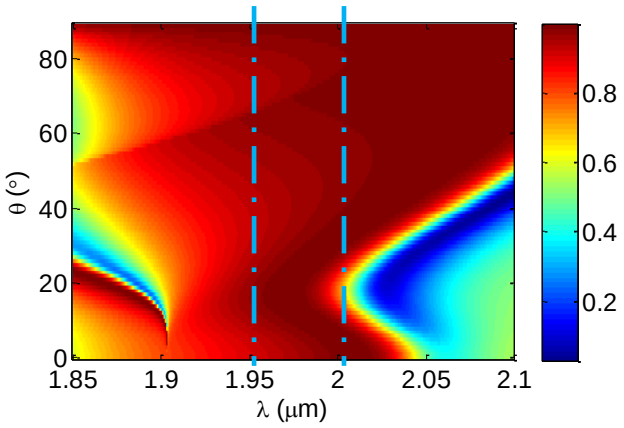

Figure 2.3 Reflectance map R_0 (λ, θ) for a silicon TE-ODR. Profile parameters are d_g = 0.989 μm, d_{wg} = 0.15 μm, Λ = 0.816 μm and F = 0.573.

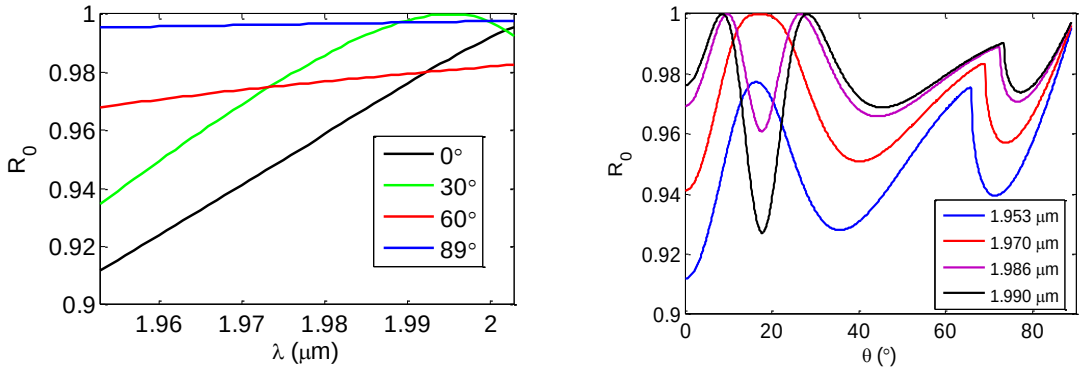

(a) (b)

Figure 2.4 Reflectance spectra for a silicon TE-ODR. Reflectance spectra at example incident angles in the 1.95-2.05 μm wavelength band (a), and reflectance spectra at example incident wavelengths in the 0-90 degree angular band (b).

Physical insight into the formation of the all-angle high reflectance can be gained by plotting the angular spectrum of the zero-order transmittance on a log scale. Figure 2.5 demonstrates that two resonances at 10 and 26 degrees, respectively, work together to support a nearly flat angular band at λ=1.985 μm. This is analogous to the 600-nm band high-TE reflector (normal incidence only) discussed above. By subsequently numerically tracking the resonance locations, the resonances are found to be TE_1-like for θ=10° with mixed modes for θ=26° comprising ~TE_0 in the waveguide layer and ~TE_1 in the grating layer consistent with computed mode patterns as shown in Figure 2.6.

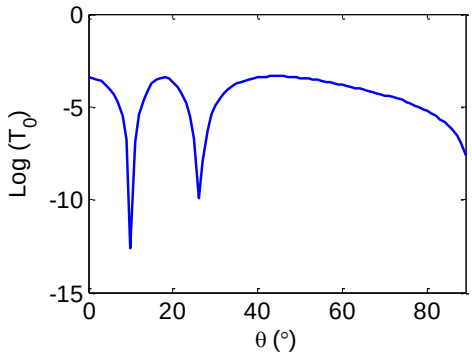

Figure 2.5 Angular spectrum of log (T_0) at λ=1.985 μm.

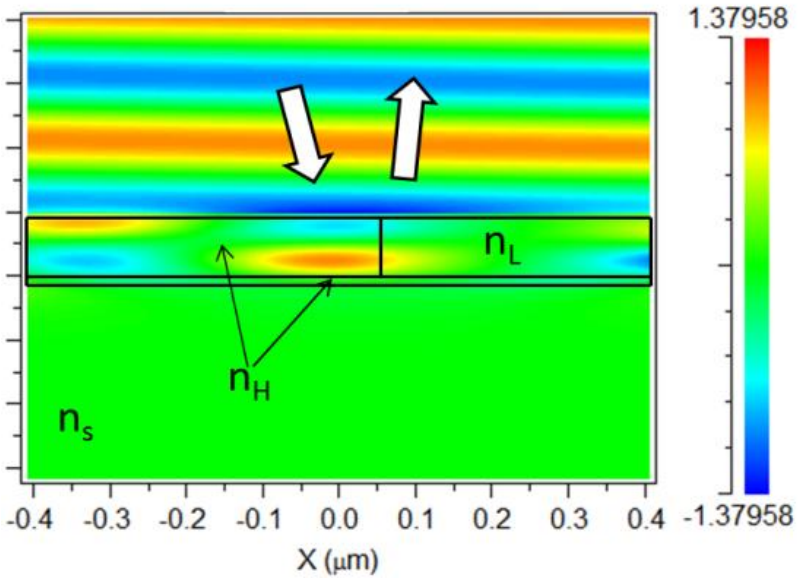

(a)

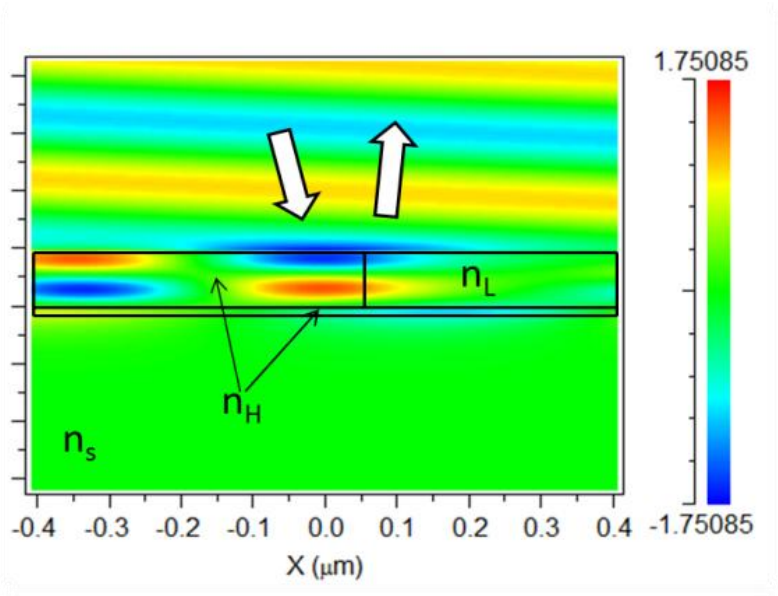

(b)

Figure 2.6 Electric field distribution patterns in the resonant reflector at λ=1.985 μm, θ=10° (a) and θ=26° (b).

Above, a silicon grating waveguide exhibiting 50nm-band omnidirectional reflectance larger than 95% is presented and discussed in detail. Such structures can further be optimized by using higher refractive index like germanium, because stronger refractive index contrast leads to wider resonance. The designed germanium grating waveguide has 66 nm bands for omnidirectional reflectance larger than 95%, and 20 nm bands for omnidirectional reflectance larger than 99% under TE polarization—see Figure 2.7.

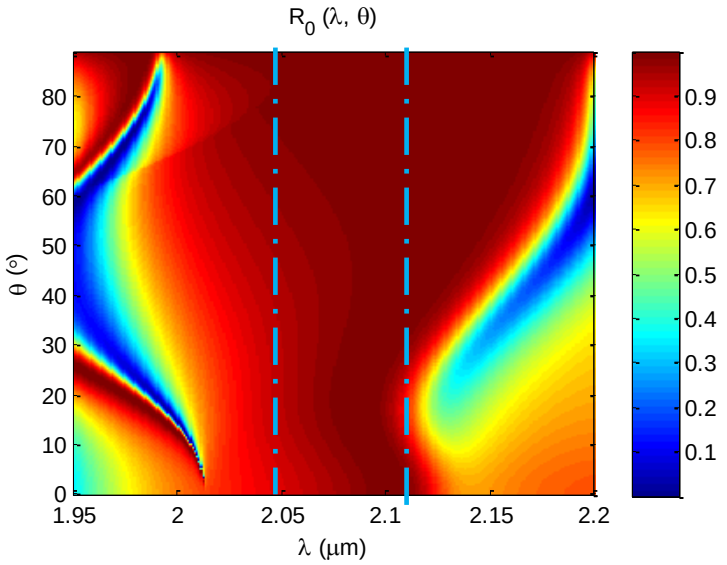

Figure 2.7 Reflectance map R_0 (λ, θ) for a germanium TE-ODR. Profile parameters are d_g = 0.87 μm, d_{wg} = 0.426 μm, Λ = 0.829 μm and F = 0.494.

2.2.2. TM Omnidirectional Reflectors

Similarly, TM omnidirectional reflectors are also designed. Generally speaking, GMR based reflector has wider band for TM polarization. This is also applicable for ODR devices. A generated TM ODR using germanium has the following parameters: d_g = 0.808 μm, d_{wg} = 0.931 μm, Λ = 1.162 μm and F = 0.571. It has a 244 nm band for R_0 (λ, θ) larger than 95% and 42 nm band for R_0 (λ, θ) larger than 99%, as shown in Figure 2.8.

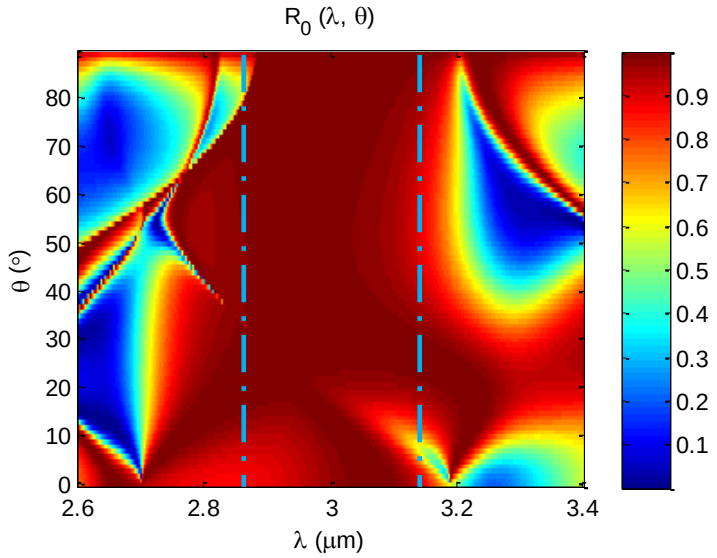

Figure 2.8 Reflectance map R_0 (λ, θ) for a germanium TM-ODR. Profile parameters are d_g = 0.808 μm, d_{wg} = 0.931 μm, Λ = 1.162 μm and F = 0.571.

In summary, one-dimensional subwavelength silicon & germanium grating providing high omnidirectional reflectivity within specific band are designed for both TE and TM polarizations. Note that the GMR location is parametrically scalable, for instance, the center wavelength could be scaled from 2μm to 1.55 μm for optical communication applications. Polarization-independent ODRs based on GMR are possible by using two-dimensional structures as well as properly designed one-dimensional periodicities.

CHAPTER 3

GUIDED-MODE RESONANCE ABSORBERS

These years, thin-film solar-cell technology grasps much attention as it provides a promising solution to lower the cost [26-29]. High optical absorption efficiency is of prime importance for reducing production cost per unit output. In the past, GMR devices have been designed most often for reflection, transmission, and polarization-control applications [8, 30]. However, by using absorbing material such as hydrogenated amorphous silicon (a-Si:H), GMR structures can also be engineered to be efficient absorbers for solar cells [31, 32].

In addition, light absorbers are important for many other applications like cross-talk reduction in optoelectronic devices and thermal light emitting sources. Although many efforts have been made to achieve high absorption, they are generally limited to achieving absorption at specific incidence angles or for narrow bandwidths [33-36]. There are great demands for wideband omnidirectional reflectors with simple structure that is easy to fabricate and low cost.

In this chapter, GMR absorbers designed for both solar cells and omnidirectional absorption applications will be presented, including design principles and simulation results.

3.1 Guided-Mode Resonance Absorption

Leaky-mode resonant devices are conventionally applied as high reflectors, polarizers, antireflection elements, extremely narrow filters and polarization-independent elements. All these devices are designed and fabricated based on lossless material. However, leaky-mode resonances can also be properly engineered in lossy materials to achieve high absorption, which provides a low-cost solution for optical absorption. Firstly, we will study the relation between GMR reflection and absorption through an example.

Ding reported resonant leaky-mode TE and TM silicon based high reflectors in [8]. Below we study one of these examples through artificially giving the lossless material a nonzero extinction coefficient. In this way, leaky-mode resonant reflection and absorption are reasonably connected. Figure 3.1 (a) shows the device has a ~600nm band with reflection efficiency larger than 99% [8]. This broad band feature is a combined result of two resonances which are shown in Figure 3.1 (b). Assuming the material to be lossy with complex refractive index, Figure 3.1 (c) presents the absorption efficiency resulting from n_{Si}=3.48+j0.8. It is observed that GMR structure absorbs ~80% light by localizing light therefore enhancing the interaction of light and material. Further calculation shows that the absorption enhancement due to GMR is determined by both radiation coupling rate and internal loss rate. In other words, when they equal to each other, the maximum absorption enhancement is achieved. This condition is named *critical coupling* in literature [37-39]. Figure 3.1 (d) supports this argument by showing the average absorbance in 1.4μm~2.2μm band as a function of extinction coefficient κ. The critical coupling condition is satisfied at κ=0.8.

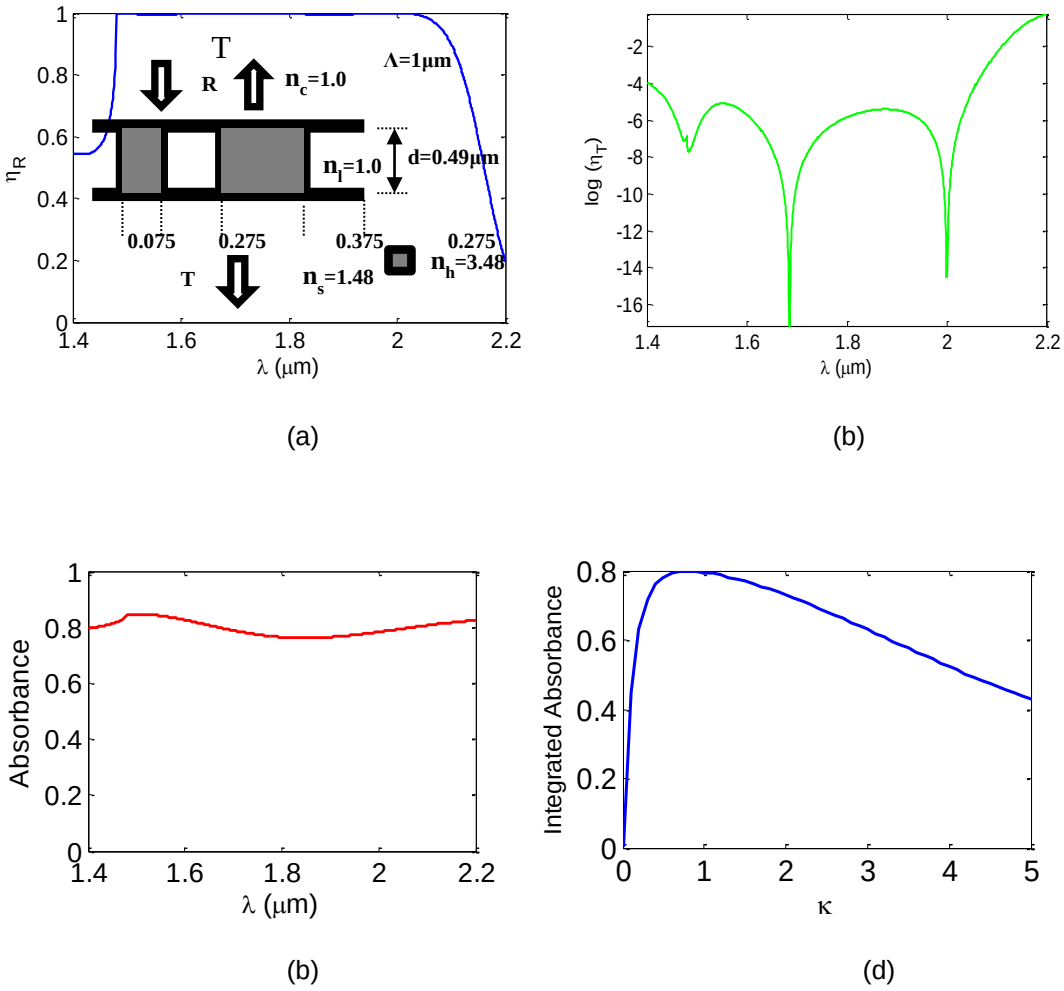

Figure 3.1 A GMR based TE reflector with 600nm band. Reflectance of the GMR device and profile parameters are shown in (a), transmittance of the device on a log scale in (b), absorption efficiency when assuming n_{Si}=3.48+j0.8 in (c), and integrated absorbance as a function of extinction coefficient κ in (d).

3.2 GMR Absorption Enhancement Engineering for Solar Cells

3.2.1 Introduction

Efficient use of light is required in many practical applications including photodetectors and solar cells. In particular, to advance progress in clean energy and to protect the global environment, thin-film solar-cell technology is of interest as a promising alternative. High optical absorption efficiency is important to reduce production cost per unit output. Enhanced absorption of the solar spectrum can be accomplished by periodic and random surface texturing to improve light trapping [40]. For example, numerous researchers used classic diffraction gratings to elongate the effective path length of the light in the absorbing medium [41, 42]. Additionally, nanopatterned films in waveguide geometry including one-dimensional (1D) and two-dimensional (2D) subwavelength photonic lattices are under development for the same reason. These compact elements exhibit strong resonance effects that originate in leaky modes undergoing a guided-mode resonance (GMR) inside the layer [43-46].

Investigation of conditions under which total or near-total absorption is achieved is an interesting associated study with analogous applications. Total absorption in narrow spectral bands in metallic periodic structures has been reported [47-49]. Clusters of silicon nanowires can provide effective antireflection across wide bands with subsequent high absorption; these structures are typically very thick [50, 51]. Similarly, it is possible to improve absorption by structuring the surface of the absorber as a pyramidal or conical profile, thus simulating a graded-refractive-index antireflection layer. These well-known structures transmit light efficiently into the underlayer across wide spectral and angular bands [52, 53].

We treat the GMR absorber structure that is schematically depicted in Fig. 3.2. It is a partially etched a-Si:H waveguide on top of a silica substrate. Hydrogenated amorphous silicon has a complex refractive index such that the resonant leaky modes generated by the periodic region are absorbed well up to the ~750 nm wavelength corresponding to a band gap energy of ~1.65 eV. This material can be made n-type or p-type for solar cell as necessary, and its optical

properties greatly depend on the H-content [54]. Figure 3.3 shows the complex refractive index we use in this thesis. In addition, the substrate silicon dioxide is also considered as dispersive $n_{sub}^2=C_1+C_2\lambda^2/(\lambda^2-C_3)+C_4\lambda^2/(\lambda^2-C_5)$, $k_{sub}=0$, in which $C_1 = 1.28604141$, $C_2 = 1.07044083$, $C_3 = 1.00585997e\text{-}2$, $C_4 = 1.10202242$, $C_5 = 100$ [55].

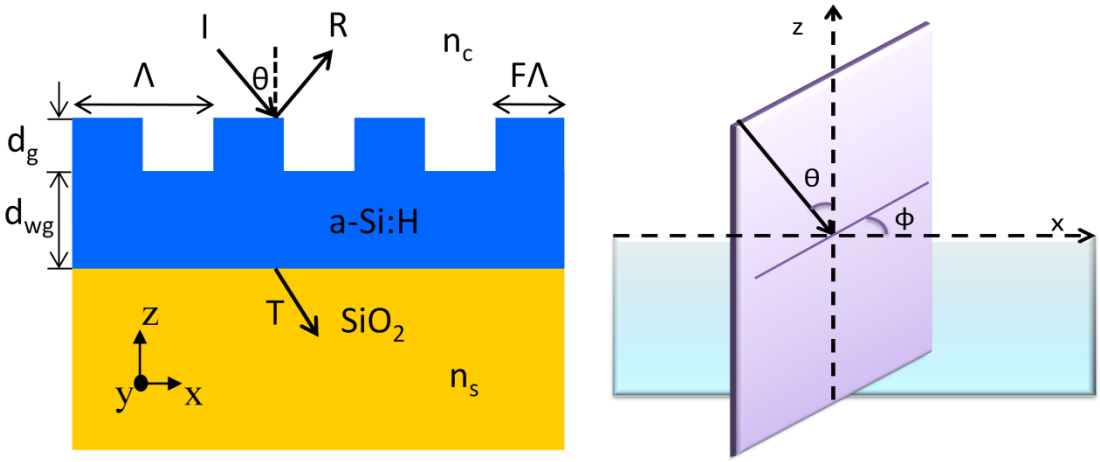

Figure 3.2 Schematic of GMR structure for solar cell. Λ, d_g, d_{wg}, and F are period, thickness, and fill factor of the a-Si:H waveguide grating, respectively.

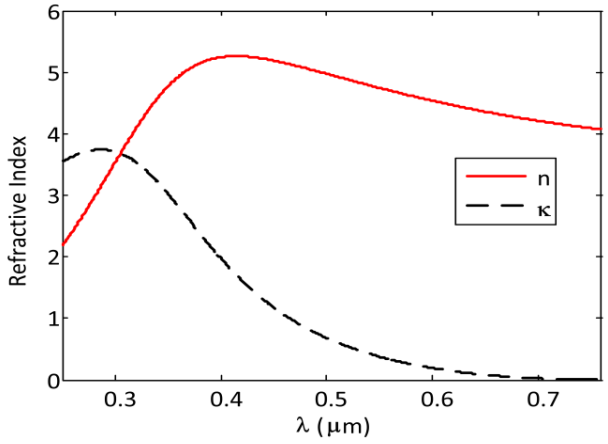

Figure 3.3 Dispersive curve of a-Si:H deposited at 300°C, H-content of ~9.5% [54].

1D grating structures for GMR-induced resonant absorption are proposed as they provide sufficient control of the Fourier harmonics affecting resonance locations while remaining

simple and amenable to fabrication. We simulate the device using rigorous coupled wave analysis (RCWA) . The absorbance is defined as

$$\mathrm{A} = 1 - (\sum_{\mathrm{i}} R_i + \sum_{\mathrm{i}} T_i) \tag{3.1}$$

in which Ri and Ti are the efficiencies of the i-th reflected and transmitted diffraction orders. Based on this core algorithm, we developed inverse numerical codes using genetic algorithms to conduct a parametric search to optimize the absorption efficiency in specific spectral bands.

3.2.2 Symmetric Structure

Generally, two parts grating (with fill factors [F, 1-F]) is referred as symmetric structure, while some four parts grating (with fill factors [F1, F2, F3, F4]) can be properly designed as asymmetric. Asymmetric GMR structures provide more dimensions for design, and also eliminate the degeneracy of symmetric structures therefore more resonances appear [30]. However, the former are simpler and more easily to be fabricated. Firstly, a symmetric example optimized by genetic algorithm is given below.

We endeavor to maximize the TM absorbance in the wavelength band of ~460-560 nm, where solar energy is mainly concentrated. The parameters suggested by the genetic algorithm are Λ=310 nm, F=0.58, d_g=90 nm, and d_{wg}=270 nm. For this period, the substrate Rayleigh anomaly occurs at $\lambda_R = n_s\Lambda$= ~481 nm below which higher-order transmitted waves begin to appear, reducing the absorption efficiency. In our example device, the transmission diffraction efficiencies for these waves are λ<0.02% for 300<λ<481 nm. For λ>481 nm, a pure zero-order GMR regime occurs, which provides an efficient interaction between the incident light and the resonant film. Figure 3.4 (a) shows that the TM polarized light is nearly totally absorbed (>98%) in the ~460-560 nm band. TE polarized light is less absorbed but still exceeding that absorbed in the corresponding planar structure across the band.

To elucidate the resonance character of the device, Figure 3.4 (b) shows the leaky-mode resonance spectral features by plotting the TM reflection spectrum of the same structure

with the extinction coefficient κ artificially set to zero. It is found that three guided-mode resonance reflection peaks occurring near 489 nm, 534 nm, and 591 nm correspond to the high absorption band in Figure 3.4 (a). As the value of κ rises and the resonant light is absorbed, the reflection peaks diminish, broaden, and shift in frequency as discussed by Shin et al [56], leading to the monotonic absorption spectrum in Figure 3.4 (a).

To evaluate the absorption in the actual solar spectrum, the absorbance A(λ) in Fig. 3 is weighed by the standard AM1.5 solar spectrum I(λ) and defined as

$$A_{ave} = \int_{300nm}^{750nm} A(\lambda) I(\lambda) d\lambda \Big/ \int_{300nm}^{750nm} I(\lambda) d\lambda \tag{3.2}$$

We find that this integrated absorbance (measuring the fraction of sunlight absorbed) is ~77% for the (optimized) TM polarization case whereas that under TE polarization is near ~55%. Figure 3.4 (c) shows that most of the unabsorbed light is reflected as zero-order diffraction. We further calculate the integrated reflectance, whose definition is analogous to Eq. 2, finding ~21% for TM polarization and ~37% for TE polarization. The unpolarized integrated absorbance across the 300-750 nm band is calculated as ~66% while the corresponding planar structure with thickness d_g+d_{wg} has ~41% absorption. Thus, this device achieves a ~60% increase relative to the unpatterned film, which is an improvement over previously reported single-layer grating design finding a ~35% increase in the 300-750 nm range [57].

As sunlight impinges on a flat surface from every direction, the angular response of the device is also examined. Figure 3.4 (d) shows that the angular aperture of the GMR absorber is wide and that it provides increasing enhancement as the angle becomes larger.

In conclusion, we applied GMR effects to enhance absorption in an ultra-thin film of amorphous silicon. A 1D photonic structure with subwavelength periodicity is designed and optimized using RCWA with a genetic algorithm for operation with the standard AM1.5 solar spectrum. For TM polarized light, this device remarkably achieves near-total absorption in a

~100 nm wide band in the center of the solar spectrum. The GMR-based solar-cell structure found has a ~60% increase in absorbance relative to a comparable planar structure. Imbuing the device with a metal reflector yields a higher integrated absorbance nearing 73%.

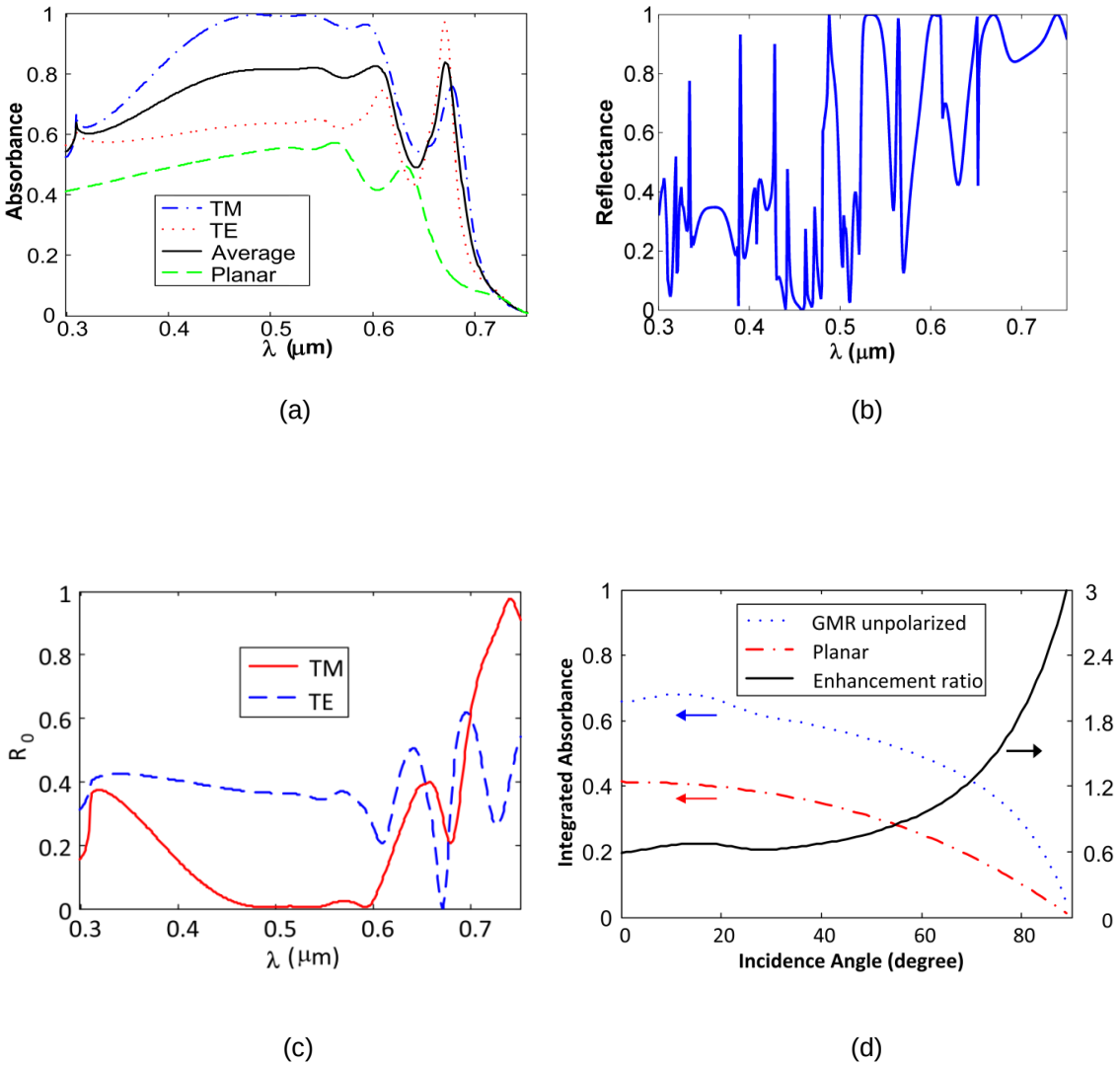

Figure 3.4 Spectral response of a GMR-based solar cell symmetric structure. Computed absorption spectra (a) at θ=0 for TE, TM, and unpolarized light and for a planar reference structure with thickness of 360 nm, zero-order normal-incidence reflection spectrum with κ=0 for TM polarization (b), zero-order reflection spectra under TM and TE polarization for κ=0 (c), and integrated absorbance and enhancement ratio of the optimized GMR absorber as a function of incidence angle (d).

3.2.3 Asymmetric Structure

Above we have mentioned that asymmetric structure can further enlarge the absorption band by eliminating the degeneracy of resonance. Asymmetric structures may be realized through using triangle shape; however, fabrication is more complicated. Another option is to fashion four-part binary grating without mirror symmetry. In addition, four parts structure provides more dimensions to control the resonance location and line-width. A polarization-independent 1D solar cell is generated by genetic algorithm shown in Figure 3.5. The fill factors are F= [0.02, 0.31, 0.37, 0.30]. In this case, the smaller a-Si:H ridge in the grating profile provides a channel for absorbing the TE polarization light, while the larger part mainly contribute to the TM polarization absorbing. This can be observed from the field pattern shown by Figure 3.6 (b) and (c). On the whole, this device absorbs ~62.4% of AM 1.5 solar energy.

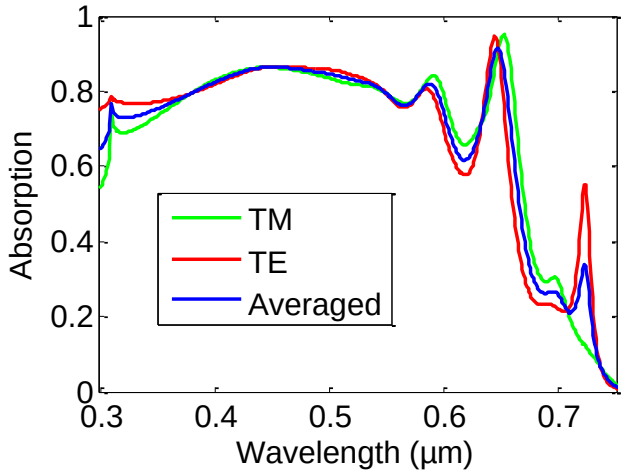

Figure 3.5 Absorption spectra of an asymmetric structure for TM, TE, and unpolarized light. Λ=310nm, d_g=90nm, d_{wg}=340nm and F= [0.02, 0.31, 0.37, 0.30].

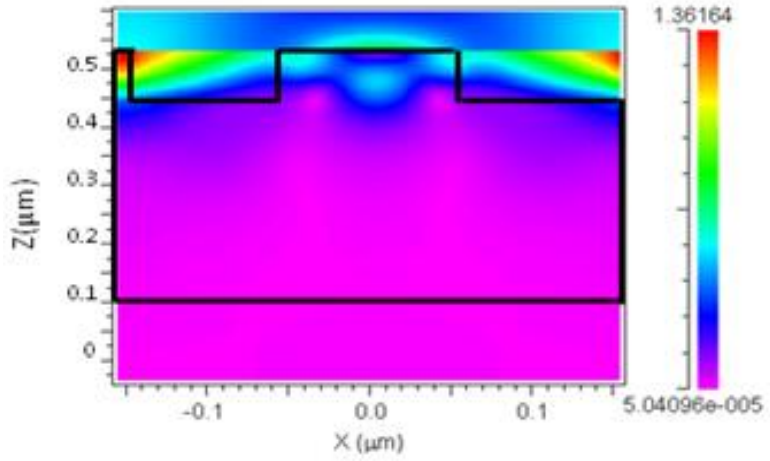

(a)

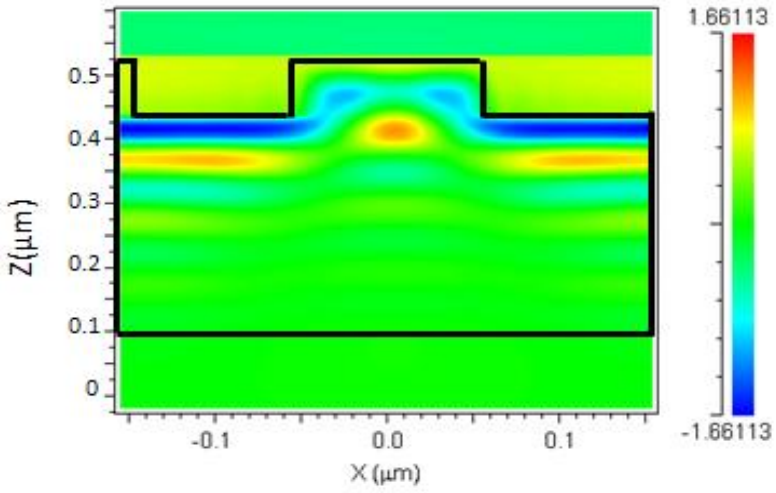

(b)

Figure 3.6 Field pattern of the polarization-independent asymmetric cell. Both electric field amplitude pattern for TE polarization at 481nm (a) and magnetic field standing wave pattern for TM polarization at 481nm (b) are shown.

3.2.4 Absorption Enhancement with Metal Reflector

The absorption efficiency can be further enhanced by adding a metal reflector on the backside of the absorbing layer to decrease the transmitted light [58]. Computed absorption spectra are shown in Figure 3.7. The integrated absorbance is increased to ~69% with a 70 nm thick Ag reflector and to ~73% with an Al reflector with the same thickness. These metal reflectors principally work for wavelengths larger than ~540 nm.

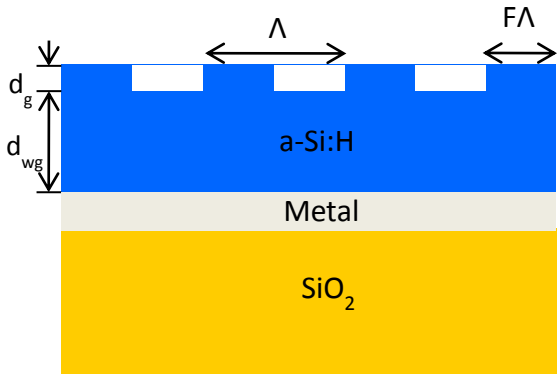

(a)

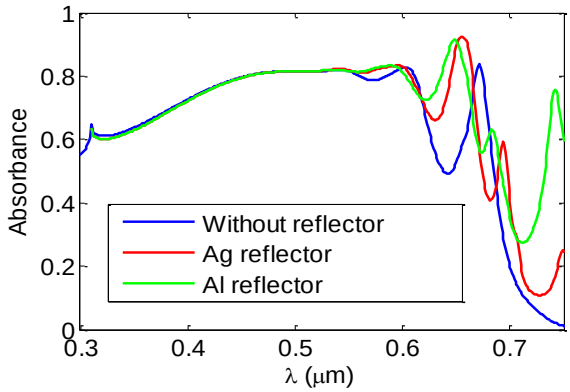

(b)

Figure 3.7 Absorption enhancement with metal reflector. Schematic of the cell (a) and absorption spectra (b) when the backside is coated with 70 nm thick Ag or Al. Spectrum without metal is plotted for comparison.

3.3 Omnidirectional Wideband GMR Absorbers

Light absorbers are important for many applications like solar cells, cross-talk reduction in optoelectronic devices and, thermal light emitting sources. Although many efforts have been made to achieve high absorption, they are generally limited to achieving absorption at specific incidence angles or for narrow bandwidths. Periodic grating structures have been proposed to absorb light but are limited to specific range of incidence directions. Total light absorption in a nanostructured metal surface has been reported but the working frequency band is narrow [59]. Deeply etched 2D gratings have also been reported for enhancing absorption in thin crystalline-silicon solar cells with ~15 μm thick films [60].

In this section, we show that near-total omnidirectional absorption of light for both TE and TM polarizations can be achieved in one guided-mode resonant grating that enhances absorption by strongly localizing the light. Also, the angle-independent thin GMR absorber (~2 μm silicon film) works near-uniformly in the wavelength range from 0.3 μm to 0.6 μm, while still remaining very simple 1D geometrical shape.

Guided-mode resonant devices have been applied as high reflectors, polarizers, antireflection elements, extremely narrow filters, and polarization-independent elements. These devices benefit from one or more aspects of the GMR effect including narrow or broad band resonance, polarization independence, full or null reflection, and high angular tolerance. In this work, we utilize these features together to realize an omnidirectional, polarization-independent, broadband absorbing device. The result shows a remarkable structure with excellent features and could potentially be useful for solar cells and other absorption applications.

3.3.1 Structure Design

The structure for omnidirectional wideband GMR absorber is similar to that designed for solar cell, as shown in Figure 3.2. The difference is that a deep resonant grating has to be adopted in order to achieve higher absorption and larger tolerance to incident angle and wavelength.

By using inverse codes incorporating RCWA and genetic algorithms, the profile parameters are determined to be Λ=0.419 μm, F=0.155, d_g=2 μm, d_{wg}=0.03 μm, and a-Si:H is adopted as absorbing material—see Figure 3.2.

3.3.2 Simulation Results

The proposed GMR absorber is investigated using hemispherical simulation. Here, we define the angle between the incidence plane and x-z plane (see Figure 3.2) as azimuthal angle φ, and the angle between incidence light beam and z-axis as incidence angle θ. Figure 3.8 exhibits a computed absorption map A(λ, θ) at φ=0, showing that the device exhibits a bandwidth of 300 nm in the chosen wavelength band spanning 0.3-0.6 μm for which all-angle incidence TE & TM light is nearly-fully absorbed.

Further calculation shows that such high absorption is also independent of the azimuthal angle. We define θ-averaged absorbance

$$[A]_\theta(\lambda,\varphi) = \frac{1}{2}\int_{-\pi/2}^{\pi/2} \cos\theta\, A\,(\lambda,\theta,\varphi)d\theta \tag{3.3}$$

which is plotted in Figure 3.9.

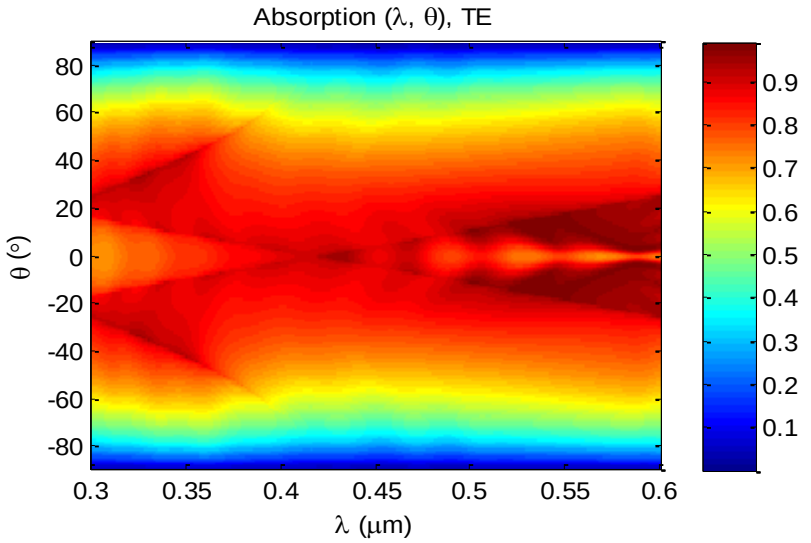

(a)

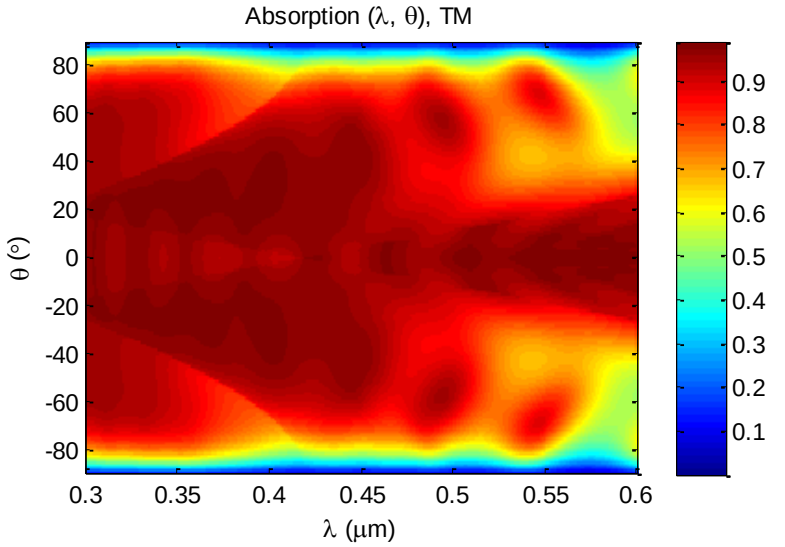

(b)

Figure 3.8 Absorption map A (λ, θ) at φ=0 under TE polarization (a) and TM polarization (b).

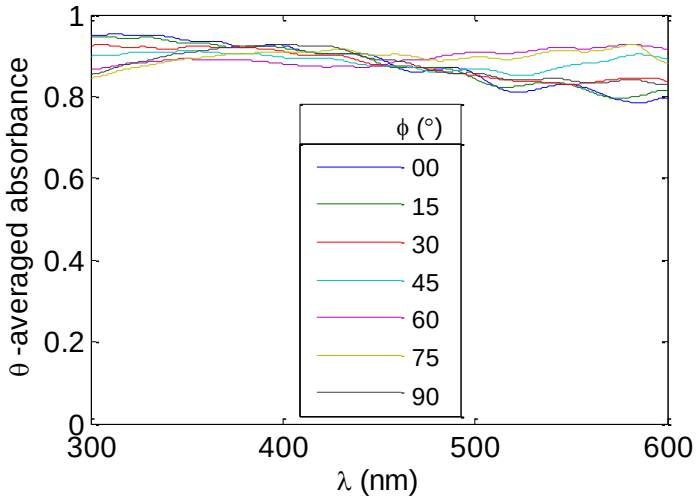

Figure 3.9 θ-averaged absorbance for wavelength in the 300-600 nm range and φ in the 0-90 degree range. Incident light is TM polarized.

It is observed that the device shows very good uniformity both for azimuthal angle and frequency. In order to compare GMR absorber with planar structure, θ and λ averaged absorbance is defined as

$$[A]_{\theta,\lambda}(\varphi) = \frac{1}{0.3\ \mu m}\int_{0.3\ \mu m}^{0.6\ \mu m} [A]_{\theta}(\lambda,\varphi)\, d\lambda \tag{3.4}$$

In Figure 3.10, θ and λ averaged absorbances for both TM and TE are plotted. One may note that the device performs well for both polarizations: above 80% light is absorbed for each. Planar structure with the same thickness has only ~52% light absorbed. Finally, averaged absorbance for θ, λ and φ is given by

$$[A]_{\theta,\lambda,\varphi} = \frac{1}{2\pi}\int_{0}^{2\pi} [A]_{\theta,\lambda}(\varphi)\, d\varphi \tag{3.5}$$

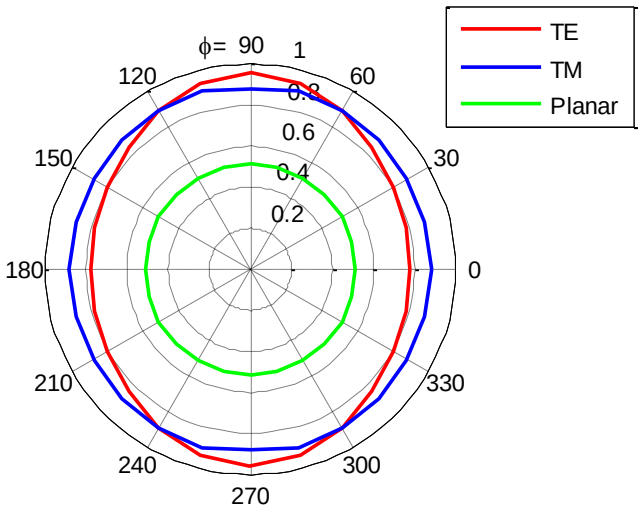

Figure 3.10 θ and λ averaged absorbance $[A]_{\theta,\lambda}(\varphi)$ for TE and TM polarizations. Absorbance for planar structure is also computed for comparison.

By averaging two polarizations, the GMR grating absorbs 87% of the hemispherical incidence light as represented by Eq. 3.5; while the planar structure with the same thickness and hence 6 times the amount of material absorbs only 52%. In other words, the GMR absorber increases the absorption by 167% while using only 16% of the material volume used in planar structure.

As discussed above, the GMR absorber greatly enhances the absorption for all incident light, independent of incidence plane and incidence angle. In a sense, it is also independent of incidence wavelength. All of these good features are of great significance for absorption applications. The grating depth is designed properly in thickness in order to make the resonance density larger. The resonances localizing in the grating remarkably increase the interaction time of photons and matter, therefore enhance the absorption and decrease the reflection. This is why GMR absorber exhibits broad band in both azimuthal and incidence angles, as well as wavelength.

Figure 3.11 displays how the grating depth influences the absorbance. For simplicity, we limit the calculations to TM polarization and θ=0, φ=0. Note that even though the 4-μm-depth

grating has better performance, the enhancement is not very significant comparing with 2-μm-depth grating. Thus, 2 μm is a promising thickness.

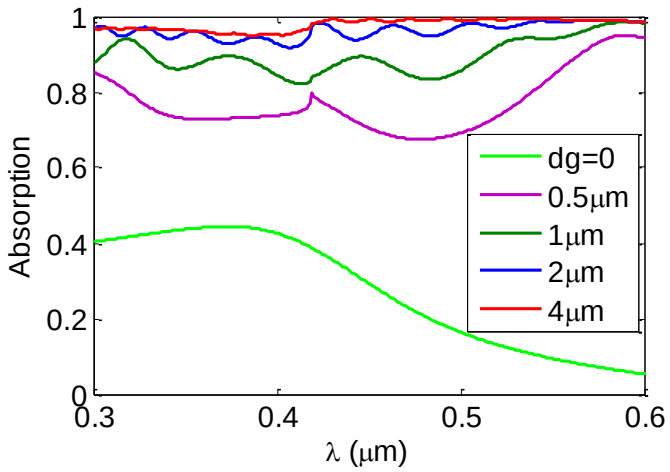

Figure 3.11 Absorption increases as the grating thickness increases, where θ=0, φ=0 and TM polarization are assumed.

3.3.3 Tolerance Analysis

Generally GMR devices are very sensitive to profile parameters and incidence wavelength or angle. This is the principle used in high-accuracy GMR sensors. However, in some other applications like broadband reflectors and absorbers, good tolerance is desirable. We demonstrate through simulations that the absorber proposed in this paper has very good tolerance to incidence wavelength and angles. Moreover, it is also not sensitive to the profile parameters as Figure 3.12 (a) and (b) present. It is shown that the value of $[\mathrm{A}]_{\theta,\lambda}(\varphi = 0)$ is quite robust near F=0.155 and Λ=0.419 μm.

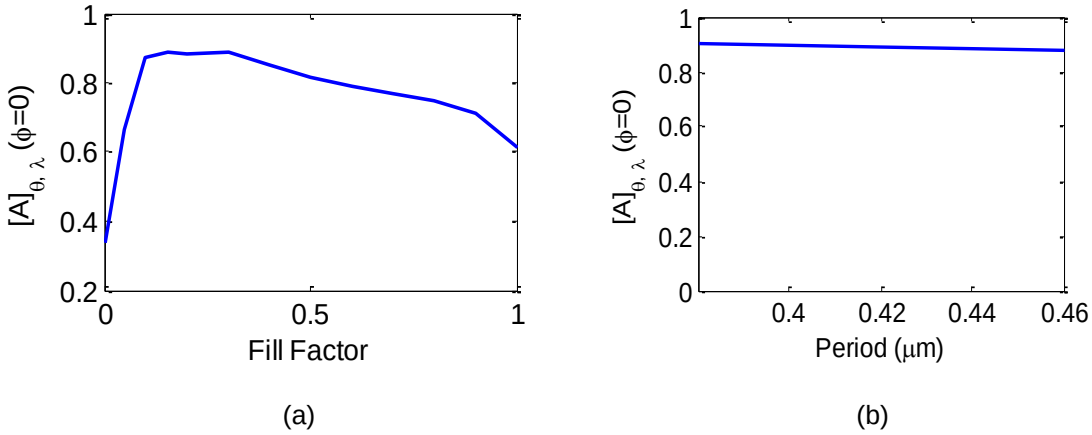

(a) (b)

Figure 3.12 Omnidirectional absorber's tolerance to the grating fill factor and period, where θ=0, φ=0 and TM polarization are assumed.

In summary, we designed an omnidirectional wideband absorber with excellent performance and good tolerance to profile parameters based on guided-mode resonance.

CHAPTER 4

GUIDED-MODE RESONANT PHOTONIC SENSORS

The market has great demands for cost-effective and reliable sensor technologies for applications in homeland security, biomedicine and environmental monitoring. Ultrasensitive and label-free GMR biosensors are in the early stages of commercial development, and the subject of much research in both academia and industry.

4.1 Principle of GMR Sensors

The label-free resonant photonic biosensors [61, 62] work based on guided-mode resonance: when a broadband light source illuminates the GMR sensors, a specific wavelength and angle of light is totally reflected, while the nearby band is fully or partly transmitted. This reflection peak wavelength or angle is then tracked during biomedical or environmental detections. Figure 4.1(a) schematically shows the binding interaction of an immobilized receptor with an analyte; it can be monitored, without use of chemical tags, by following the corresponding resonance wavelength shift with a spectrometer as denoted in Figure 4.1(b). Since the resonance layer is polarization-sensitive, separate resonance peaks occur for incident TE and TM polarization states. These separate resonances are helpful for determining several unknowns in one channel. The sensor element can be prepared with standard surface chemistries to covalently attach a selective detection layer such as antibodies or other alternatives for different applications.

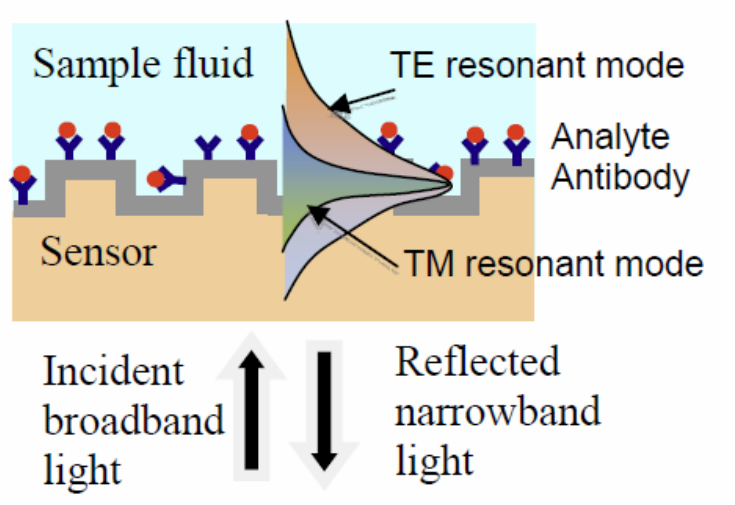

(a)

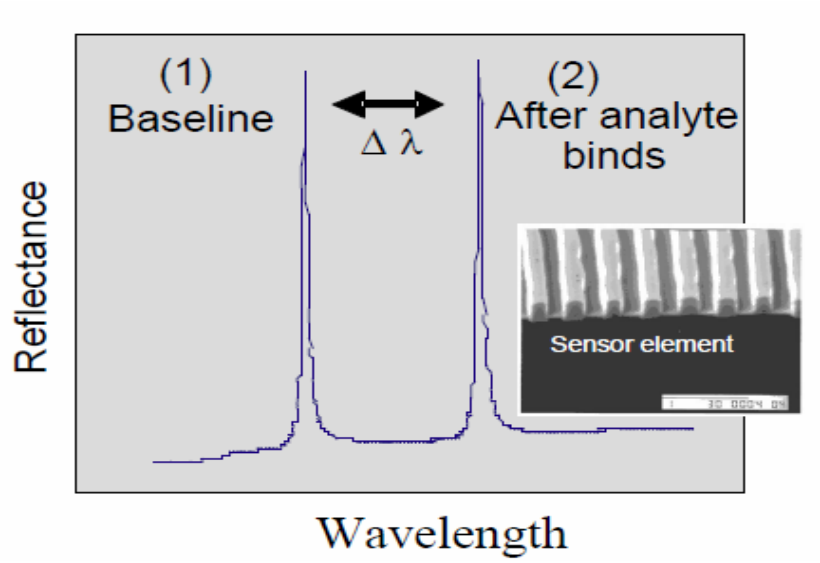

(b)

Figure 4.1 An example of GMR sensor: schematic (a) and principle (b). Binding events occurring at the sensor surface produce resonance-peak shifts that can be tracked in real time [62].

There are two basic ways tracking the resonance location: angle based and wavelength based. The former tracks the resonance angular shift by using fixed wavelength light source, while the latter tracks the resonance spectral shift by using fixed incident angle light source.

When light illuminates a periodic waveguide element, a guided-mode resonance can occur at a specific frequency and angle. The element has a bio-selective layer used to attract the target analyte; as a result, the sensor parameters change whereby a resonance shift is detected. However, the experimental environment contains noise, including temperature fluctuations, which can also cause resonance location shifts through changing the background refractive index. For this class of ultrasensitive sensor devices, it is of great significance to differentiate the analyte influence from background noise. Therefore, resonant photonic biosensor back-fitting method, a powerful mathematical model, is proposed to fulfill this objective.

4.2 Back-Fitting Model

The back-fitting model is used to do the post analysis for experimental data. As we mentioned above, the measured resonance shift could be caused by detecting objective or background noise. By using the model, they can be differentiated clearly. As this model greatly improves the accuracy of the sensor, it is recognized as important as the data collection. An example is given below for demonstrating the validity and capability of this model.

Generally, the back-fitting model starts from a given experimental data that shows the TE and TM resonance shifts, for instance, Figure 4.2. In order to back-fit the data, both TE and TM resonance shift maps are needed. But before mapping, the initial resonance locations have to be found first. In summary, there are three steps need to be performed.

1. Find the initial resonance location without detecting layer and without any interference from background; this initial data will be the start point of next step--mapping.
2. Map the resonance shifts as function of surface and bulk refractive index changes.
3. Use the maps to back-fit the experimental results. In this step, the program looks for the points that fit the TE and TM resonance shift respectively. Then it compares them and finds the solution that fits both TE and TM shifts.

Figure 4.2 illustrates the spectral resonance shifts due to the binding of detecting objective. In this case, TM polarized reflected wave peak and TE polarized null are monitored. At time 0-49 minutes, it was a baseline measurement. The sample was introduced at t=50 min and then washed at t=132 min. For t=51-127 min, the resonance shifts are obviously observed fluctuating around 50 pm, which is extremely small indicating high sensitivity of the sensor. As discussed above, dual polarization detection was applied for the purpose of differentiating detected antigen from background noise. There are two known data sets: TE and TM resonances shift. They are used to determine two unknown data sets: background refractive index change and bio-selective layer refractive index change. The final back-fitted results are shown in Figure 4.3. It demonstrates that the background refractive index is not changing but the biolayer is changing, which means antigen has been detected. This matches exactly as what we have performed during experiment.

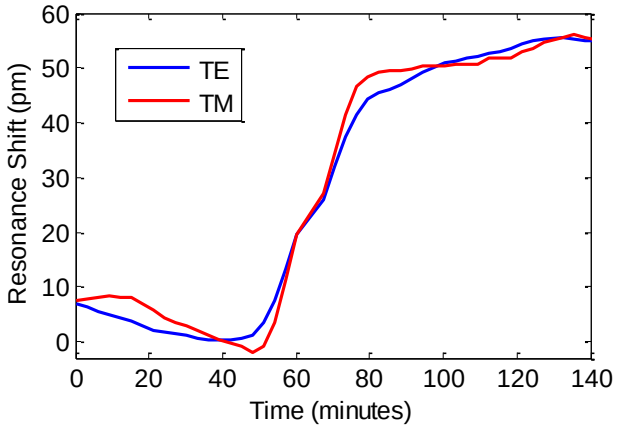

Figure 4.2 Experimental spectral resonance shifts.

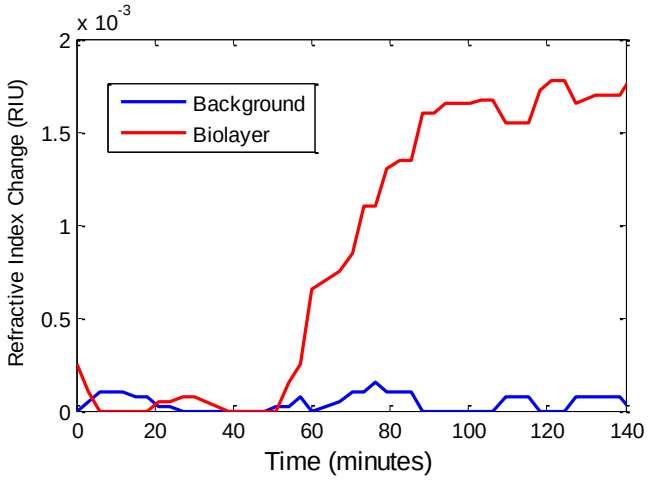

Figure 4.3 The back-fitted results showing antigen detected

In this chapter, we have demonstrated a valid, fast and economical method to differentiate the biochemical target from outside environmental disturbers for resonant photonic biosensors. This method has potential for determining biolayer thickness and refractive index as well as simultaneous background index variations in a single channel, minimizing the need for adjacent reference cells.

CHAPTER 5

EXTREMELY NARROWBAND GMR FILTERS

5.1 Simulation and Design

Above we discussed resonant photonics sensors, which work based on tracking the GMR location. The resonance line width is another important factor that affects the performance of this sort of sensors. Resonant peaks or nulls with narrow linewidths are more easily monitored than the ones with wide linewidths. In addition, narrow linewidth filters are also applied in other areas such as extremely narrow single wavelength light source generation. In this chapter, we introduce a GMR device showing extremely narrow linewidth of ~10 pm.

The structure is designed to be three layers, a SiO_2 waveguide grating on top of a homogeneous HfO_2 layer. Figure 5.1 shows the structure. The substrate of this device is glass which is not shown in the figure. Parameters are: period=450.8 nm, HfO_2 layer thickness= 200 nm, SiO_2 homogeneous layer thickness= 210 nm, grating thickness=30 nm, and fill factor= 0.5. The working wavelength is around 780 nm at normal incidence in TE polarization, where the refractive index of HfO_2 is 1.979 and SiO_2 is 1.46. As shown in Figure 5.2, the resonance width is extraordinarily narrow—measured Full Width at Half Maximum (FWHM) is 8.6 pm and resonance peak is at 780.204 nm. Moreover, the resonance location shift of the device is linear as the incident angle changes, as presented by Figure 5.3. This is good for compensating estimation in practice as the real device has unavoidable fluctuation.

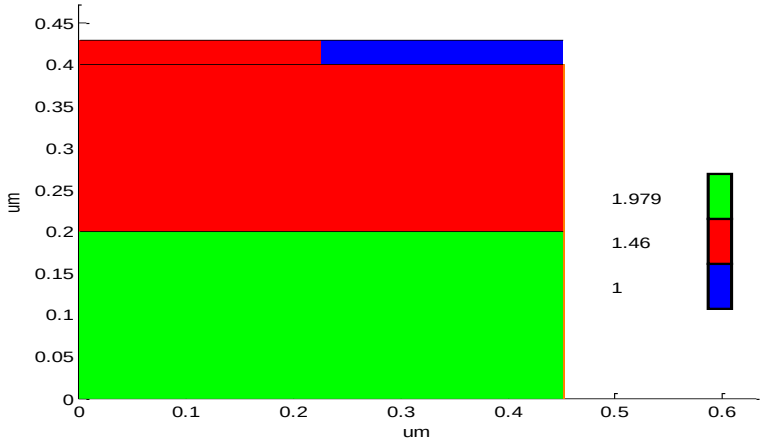

Figure 5.1 Schematic of the GMR extremely narrowband filter.

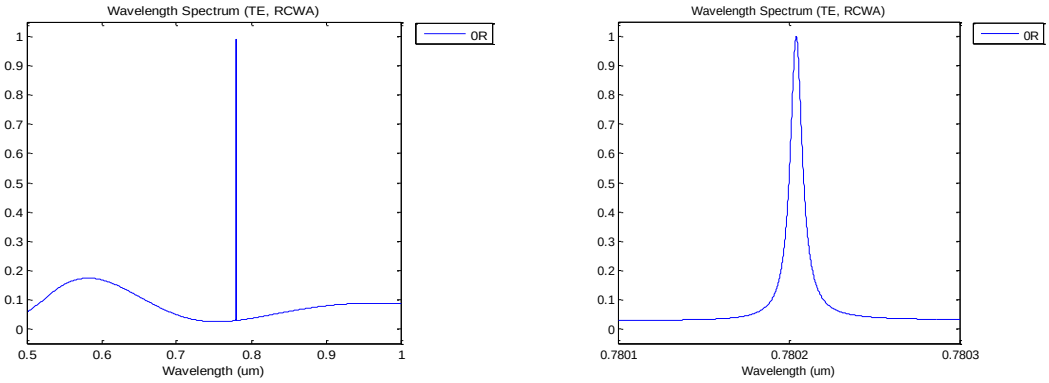

(a) (b)

Figure 5.2 Zero-order reflection spectra of the GMR filter. Both 0.5-1μm band (a) and enlargement at resonance center (b) are plotted.

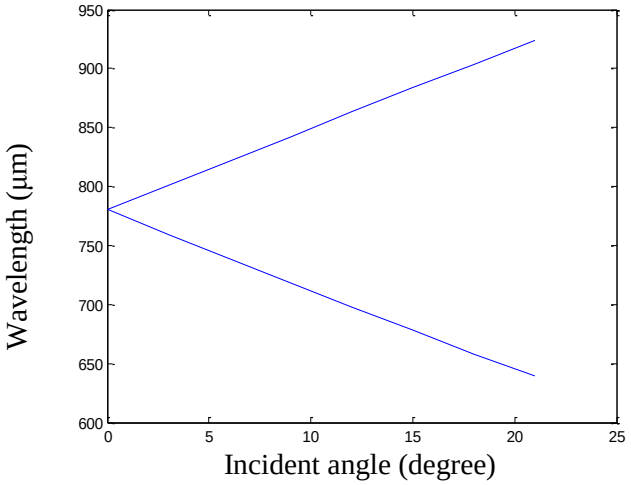

Figure 5.3 Dispersion of resonance location.

CHAPTER 6

CONCLUSIONS

6.1 Summary

This thesis mainly presents four types of GMR-based devices, which are designed using powerful inverse codes incorporating profile parameter search into diffraction efficiency calculations. These devices include omnidirectional reflectors, wideband omnidirectional absorbers, photonic biosensors, and extremely narrowband filters.

It is the first attempt to design omnidirectional devices based on guided-mode resonance. Several simple and easily fabricated omnidirectional reflectors are proposed. One of them has an angle-averaged omnidirectional reflectivity of >95% across a ~244 nm band under TM polarization. The designed GMR-based omnidirectional absorbers also show good performance: the simple amorphous silicon waveguide grating absorbs light nearly totally in the ~ 0.3-0.6 μm wavelength band for all incidence angles independent of polarization.

Besides, GMR based waveguide gratings, symmetric and asymmetric, for enhancing the absorption in solar cells are also designed and discussed. It is concluded that asymmetric structure affords more channels for enhancing absorption and back metallic reflector helps to further increase absorbance. Our grating design shows great enhancement up to 60% comparing with an equivalent unpatterned structure.

A back-fitting model is developed for improving the accuracy of GMR based biosensors. This model is proved to be fast and valid, as well as economical. Finally, a simple GMR filter exhibiting extremely narrow linewidth is discussed.

6.2 Future Work

As first reported GMR omnidirectional reflectors, they are limited to one polarization either TE or TM. However, it is possible to design polarization independent omnidirectional reflectors by using asymmetric binary gratings or two dimensional structures. The spectral band of these devices could also be widened if better parameters are found. In addition, fabrication and experimental measurement are in progress.

REFERENCES

[1] R. Magnusson, M. Shokooh-Saremi, K. J. Lee, J. Curzan, D. Wawro, S. Zimmerman, W. Wu, J. Yoon, H. G. Svavarsson and S. H. Song, "Leaky-mode resonance photonics: an applications platform", Proc. SPIE 8102, 810202 (2011).

[2] R. W. Wood, "Remarkable spectrum from a diffraction grating," Philos. Mag. 4, 396–402 (1902).

[3] A. Hessel and A. A. Oliner, "A New Theory of Wood's Anomalies on Optical Gratings," Appl. Opt. 4, 1275-1297 (1965).

[4] S. S. Wang, R. Magnusson, J. S. Bagby, and M. G. Moharam, "Guided-mode resonances in planar dielectric-layer diffraction gratings," J. Opt. Soc. Am. A 7, 1470–1474 (1990).

[5] R. Magnusson and S. S. Wang, "New principle for optical filters," Appl. Phys. Lett, 61, 1022–1024, (1992).

[6] S. S. Wang and R. Magnusson, "Theory and applications of guided-mode resonance filters," Appl. Opt. 32, 2606-2613 (1993).

[7] S. S. Wang and R. Magnusson, "Multilayer waveguide-grating filters," Applied Optics, vol. 34, pp. 2414–2420, May (1995).

[8] Y. Ding, and R. Magnusson, "Resonant leaky-mode spectral-band engineering and device applications," Opt. Express 12, 5661-5674 (2004).

[9] Y. Ding and R. Magnusson, "Band gaps and leaky-wave effects in resonant photonic-crystal waveguides," Opt. Express 15, 680-694 (2007).

[10] R. Magnusson and M. Shokooh-Saremi, "Physical basis for wideband resonant reflectors," Opt. Express 16, 3456-3462 (2008).

[11] T. K. Gaylord and M. G. Moharam, "Analysis and applications of optical diffraction by gratings," Proc. IEEE Vol. 73, Iss. 5, pp. 894–937 (1985).

[12] M. Shokooh-Saremi and R. Magnusson, "Particle swarm optimization and its application to the design of diffraction grating filters," Opt. Lett. 32, 894-896 (2007).

[13] H. Shim, J. Lee, F. Lee, and B. Jun "Optimal design of frequency selective surface by genetic algorithm", International Journal of Precision Engineering and Manufacturing, Vol.11, Iss.5, pp.725-732 (2010).

[14] S. Tibuleac, D. Shin, R. Magnusson, and C Zuffada, "Guided-mode resonance filters generated with genetic algorithm," Technical Digest of the OSA Topical Meeting on Diffractive Optics and Micro-Optics, pp.24-26, Kona, Hawaii, June 8-11 (1998).

[15] W. Wu and R. Magnusson, “Omnidirectional Reflector Using Guided-Mode Resonance in a Subwavelength Silicon Grating Under TE Polarization,” Optical Society of America Frontiers in Optics, OSA’s 95th Annual Meeting, San Jose, California, October 16–20 (2011).

[16] V. Kochergin, “Omnidirectional optical filters,” Kluwer Academic Publishers, Norwell, Mass. (2003).

[17] M. Shokooh-Saremi and R. Magnusson, "Leaky-mode resonant reflectors with extreme bandwidths," Optics Letters, vol. 35, no. 8, pp. 1121-1123, April 15, 2010.

[18] C. Tsai, S. Yang, Y. Lee, J. Chang, and M. Wu, “Omnidirectional Reflector Based on Dual Effect of Leaky Mode Resonance and Surface Plasmon Resonance,” 216th ECS Meeting, MA2009-02, Vienna, Austria, October 4 -9 (2009).

[19] Y. Fink, J. N. Winn, S. Fan, C. Chen, J. Michel, J. D. Joannopoulos, and E. L. Thomas, “A dielectric omnidirectional reflector,” Science 282, 1679-1682 (1998).

[20] J. K. Kim, T. Gessmann, E. F. Schubert, J. Q. Xi, H. Luo, J. Cho, C. Sone, and Y. Park, “GaInN light-emitting diode with conductive omnidirectional reflector having a low-refractive-index indium-tin oxide layer,” Appl. Phys. Lett. 88, 013501 (2006).

[21] J. K. Kim, H. Luo, Y. Xi, J. M. Shah, T. Gessmann, E. F. Schubert, "Light extraction in GaInN light-emitting diodes using diffuse omnidirectional reflectors," J. Electrochem. Soc. 153, G105-G107 (2006).

[22] T. Gessmann, Y.-L. Li, E. F. Schubert, J. W. Graff, J. K. Sheu, "GaInN light-emitting diodes with omni directional reflectors," Proc. SPIE (2003) pp. 139-144.

[23] S. Kim and C. K. Hwangbo, "Design of Omnidirectional High Reflectors with Quarter-Wave Dielectric Stacks for Optical Telecommunication Bands," Appl. Opt. 41, 3187-3192 (2002).

[24] S. S. Lo and C. C. Chen, "Air-core hollow optical waveguides with omnidirectional reflectors," Opt. Eng. 45, 044601 (2006).

[25] M. G. Moharam, Drew A. Pommet, Eric B. Grann, and T. K. Gaylord, "Stable implementation of the rigorous coupled-wave analysis for surface-relief gratings: enhanced transmittance matrix approach," J. Opt. Soc. Am. A 12, 1077-1086 (1995).

[26] I. Celanovic, F. O'Sullivan, M. Ilak, J. Kassakian, and D. Perreault, "Design and optimization of one-dimensional photonic crystals for thermophotovoltaic applications," Opt. Lett. 29, 863-865 (2004).

[27] N. P. Sergeant, M. Agrawal, and P. Peumans, "High performance solar-selective absorbers using coated sub-wavelength gratings," Opt. Express 18, 5525-5540 (2010).

[28] S. B. Mallick, M. Agrawal, and P. Peumans, "Optimal light trapping in ultra-thin photonic crystal crystalline silicon solar cells," Opt. Express 18, 5691-5706 (2010).

[29] X. Li, Y. Chen, J. Miao, P. Zhou, Y. Zheng, L. Chen, and Y. P. Lee, "High solar absorption of a multilayered thin film structure," Opt. Express 15, 1907-1912 (2007).

[30] Y. Ding and R. Magnusson, "Use of nondegenerate resonant leaky modes to fashion diverse optical spectra," Opt. Express 12, 1885-1891 (2004).

[31] P. N. Saeta, V. E. Ferry, D. Pacifici, J. N. Munday, and H. A. Atwater, "How much can guided modes enhance absorption in thin solar cells?," Opt. Express 17, 20975-20990 (2009).

[32] Y. Lee, C. Huang, J. Chang, and M. Wu, "Enhanced light trapping based on guided mode resonance effect for thin-film silicon solar cells with two filling-factor gratings," Opt. Express 16, 7969-7975 (2008).

[33] D. Maystre and R. Petit "Brewster incidence for metallic gratings," Opt. Commun. 17, 196–200 (1976).

[34] M. C. Hutley and D. Maystre "The total absorption of light by a diffraction grating," Opt. Commun. 19, 431–436 (1976).

[35] J. Greffet, R. Carminati, K. Joulain, J. Mulet, S. Mainguy, and Y. Chen. "Coherent emission of light by thermal sources," Nature 416, 61–64 (2002).

[36] Y. P. Bliokh, J. Felsteiner and Y. Z. Slutsker, “Total absorption of an electromagnetic wave by an overdense plasma," Phys. Rev. Lett. 95, 165003 (2005).

[37] A. Yariv, “Universal relations for coupling of optical power between microresonators and dielectric waveguides,” Electron. Lett. 36, 321-322 (1999).

[38] Yu. P. Bliokh, J. Felsteiner, and Y. Z. Slutsker, “Total absorption of an electromagnetic wave by an overdense plasma,” Phys. Rev. Lett. 95, 165003 (2005).

[39] J. Yoon, K. H. Seol, S. H. Song, and R. Magnusson, "Critical coupling in dissipative surface-plasmon resonators with multiple ports," Opt. Express 18, 25702-25711 (2010).

[40] R. Brendel, “Thin-Film Crystalline Silicon Solar Cells,” Weinheim, Germany: Wiley-VCH (2003).

[41] M. Niggemann, M. Glatthaar, A. Gombert, A. Hinsch, and V. Wittwer, “Diffraction gratings and buried nano-electrodes—architectures for organic solar cells,” This Solid Films, vol. 451-452, pp.619-623 (2004).

[42] C. Heine and R. H. Morf, “Submicrometer gratings for solar energy applications,” Appl. Opt., vol. 34, no. 14, pp. 2476-2482, May 10 (1995).

[43] Y.-C. Lee, C.-F. Huang, J.-Y. Chang and M.-L. Wu, “Enhanced light trapping based on guided mode resonance effect for thin-film silicon solar cells with two filling-factor gratings,” Opt. Express, vol. 16, pp. 7969-7975 (2008).

[44] Y. Park, E. Drouard, O. E. Daif, X. Letartre, P. Viktorovitch, A. Fave, A. Kaminski, M. Lemiti, and C. Seassal, “Absorption enhancement using photonic crystals for silicon thin film solar cells,” Opt. Express, vol. 17, pp. 14312-14321 (2009).

[45] J. R. Tumbleston, D.-H. Ko, E. T. Samulski, and R. Lopez, “Absorption and quasiguided mode analysis of organic solar cells with photonic crystal photoactive layers,” Opt. Express, vol. 17, no. 9, pp. 7670-7681 (2009).

[46] S. B. Mallick, M. Agrawal, and P. Peumans, “Optimal light trapping in ultra-thin photonic crystal crystalline silicon solar cells,” Opt. Express, vol. 18, pp. 5691-5706 (2010).

[47] N. Bonod, G. Tayeb, D. Maystre, S. Enoch, and E. Popov, “Total absorption of light by lamellar metallic gratings,” Opt. Express, vol. 16, pp. 15431-15438 (2008).

[48] T. V. Teperik, V. V. Popov, and F. J. Garcia de Abajo, “Void plasmons and total absorption of light in nanoporous metallic films,” Physical Review B, vol. 71, pp. 085408-1–085408-9 (2005).

[49] T. V. Teperik, F. J. Garcia de Abajo, A. G. Borisov, M. Abdelsalam, P. N. Bartlett, Y. Sugawara, and J. J. Baumberg, “Omnidirectional absorption in nanostructured metal surfaces,” Nature Photonics, vol. 2, pp. 299-301 (2008).

[50] S. K. Srivastava, D. Kumar, P. K. Singh, M. Kar, V. Kumar, and M. Husain, “Excellent antireflection properties of vertical silicon nanowire arrays,” Solar Energy Materials & Solar Cells, vol. 94, pp. 1506-1511 (2010).

[51] J.-Y. Jung, Z. Guo, S.-W. Jee, H.-D. Um, K.-T. Park and J.-H. Lee, “A strong antireflective solar cell prepared by tapering silicon nanowires,” Opt. Express, vol. 18, no. S3, pp. A286-A292 (2010).

[52] D. H. Arguing and G. M. Morris, “Antireflection structured surfaces for the infrared spectral region,” Applied Optics, vol. 32, no. 7, pp. 1154-1167 (1993).

[53] H. Toyota, K. Táchira, M. Okano, T. Yotsuya, and H. Kikuta, “Fabrication of microcone array for antireflection structured surface using metal dotted pattern,” Jpn. J. Appl. Phys., vol. 40, no. 7B, pp. L747-L749 (2001).

[54] A. Fontcuberta i Morral, P. Roca i Cabarrocas, and C. Clerc, “Structure and hydrogen content of polymorphous silicon thin films studied by spectroscopic ellipsometry and nuclear measurements,” Phys. Rev. B 69(12), 125307 (2004).

[55] G. Ghosh, “Dispersion-equation coefficients for the refractive index and birefringence of calcite and quartz crystals,” Opt. Commun. 163, 95-102 (1999).

[56] D. Shin, S. Tibuleac, T. A. Maldonado, and R. Magnusson “Thin-film optical filters with diffractive elements and waveguides,” Opt. Eng., vol. 37, no. 9, pp. 2634-2646 (1998).

[57] Y. Park, E. Drouard, O. E. Daif, X. Letartre, P. Viktorovitch, A. Fave, A. Kaminski, M. Lemiti, and C. Seassal, "Absorption enhancement using photonic crystals for silicon thin film solar cells," Opt. Express 17, 14312-14321 (2009).

[58] G. Yue, O. Laura, J. M. Owens, B. Yan, J. Yang, and G. Subhendu, “Optimization of back reflector for high efficiency hydrogenated nanocrystalline silicon solar cells”, Applied Physics Letters, vol.95, no.26, pp.263501-263501-3, Dec. (2009).

[59] T. V. Teperik, F. J. García de Abajo, A. G. Borisov, M. Abdelsalam, P. N. Bartlett, Y. Sugawara, and J. J. Baumberg, "Omnidirectional absorption in nanostructured metal surfaces," Nature Photonics 2, 299 - 301 (2008).

[60] S. H. Zaidi, R. Marquadt, B. Minhas, and J. W. Tringe. "Deeply etched grating structures for enhanced absorption in thin C-Si solar cells," Photovoltaic Specialists Conference, Conference Record of the Twenty-Ninth IEEE, pp. 1290-1293, 19-24 May (2002)

[61] R. Magnusson, D. Wawro, S. Zimmerman, and W. Wu, “Biosensor technology implementing optical polarization and modal diversity for determining multiple unknowns in every channel,” 27th SBEC: Southern Biomedical Engineering Conference, International Journal of Medical Implants and Devices, vol. 5, no. 2, pp. 78, 2011.

[62] R. Magnusson, D. Wawro, S. Zimmerman, and Y. Ding, "Resonant photonic biosensors with polarization-based multiparametric discrimination in each channel," Sensors: Special Issue Optical Resonant Sensors, vol. 11, pp. 1476-1488, January 26, 2011.

BIOGRAPHICAL INFORMATION

Wenhua Wu received his Bachelor of Science degree in Optoelectronics from Huazhong University of Science and Technology, China in 2009. He finished his undergraduate thesis in Silicon Photonics and Microsystems Research Group, Wuhan National Laboratory for Optoelectronics. Since 2009, he has been a graduate research assistant in the Nanophotonics Device Group at The University of Texas at Arlington. His research interests include integrated photonics, nanophotonics resonant sensors, guided-mode resonance filters, absorption engineering in solar cells, omnidirectional reflection & absorption devices as well as diffractive optics simulation and design algorithms. He has developed simulation software implementing rigorous coupled-wave analysis and coupled-mode analysis software with graphical user interfaces. He also wrote data analysis software for Resonant Sensors Incorporated. He is a student member of the Optical Society of America and serves as peer reviewer for Optics Express.